Table 4.1.4 Maximum increase of velocity in potential flow over various two-dimensional hills with low slopes.

$$\sigma_{max} = \frac{\Delta u_{max}}{(h_{hill}/L) * u_o}$$

Hill Shape		Max slope/(h_{hill} /L) u_o	σ_{max}
Inverse Polynomial	$f = 1/[1 + (x/L)^2]$	0.56	1.0
Unsymmetric Inverse Polynomial	$f = 1/[1 + (x/L_1)^2]$, $x < 0$ $f = 1/[1 + (x/L_2)^2]$, $x > 0$	0.56, $x < 0$ $0.56(L_1/L_2)$, $x > 0$	$1/2(1 + L_1/L_2)$
Gaussian	$f = \exp[-(x/L)^2 \ln 2]$	0.71	1.13
Ramp	$f = 1/2\ 1 + \tanh(x/L)]$	0.5	0.29
Sin	$f = 1/2\ \{1 + \cos[\pi/2\ (x/L)]\}$	0.79	0.93

Note that L is chosen so that $f(x/L = 1) = 1/2$ in all cases.

If the hill is in the form of an ellipsoid, a useful approximation to many hill shapes, then Δu_{max} may also be calculated by hydrodynamic methods as shown by Hunt and Simpson (1982).

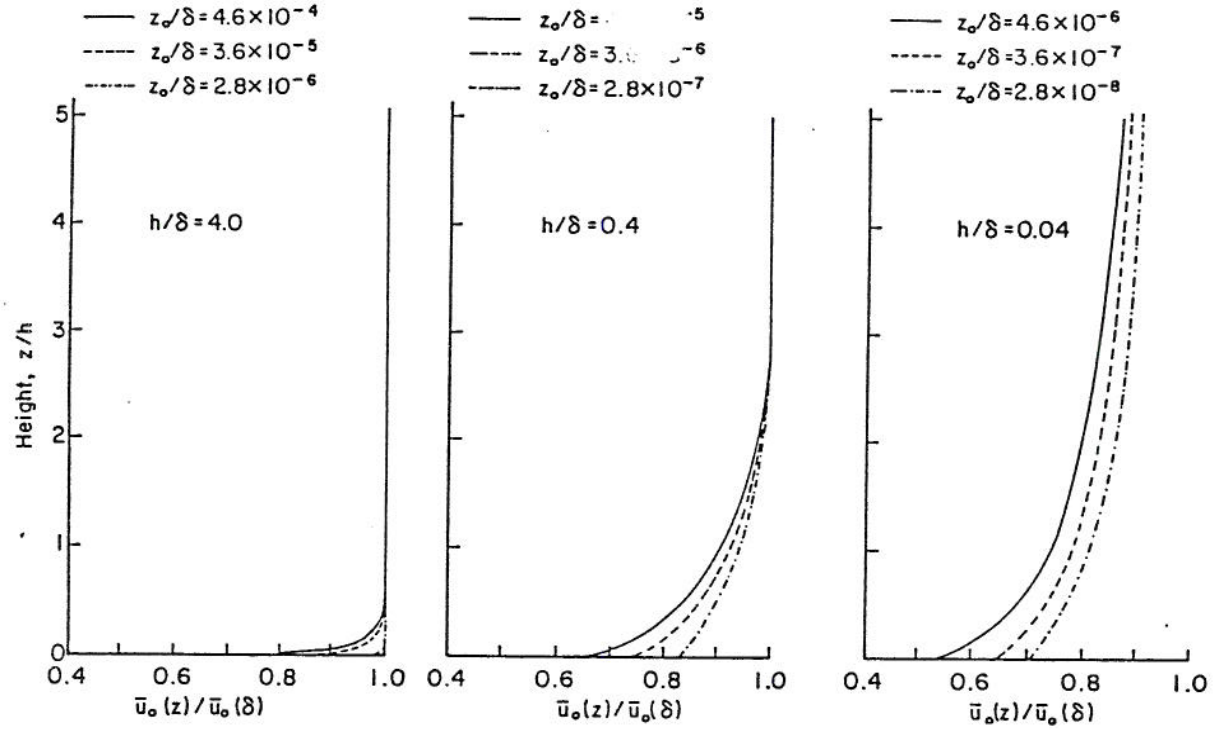

Figure 4.1.3 Approach flow velocity profiles for numerical inviscid flow calculations. (Bouwmeester *et al.*, 1978)

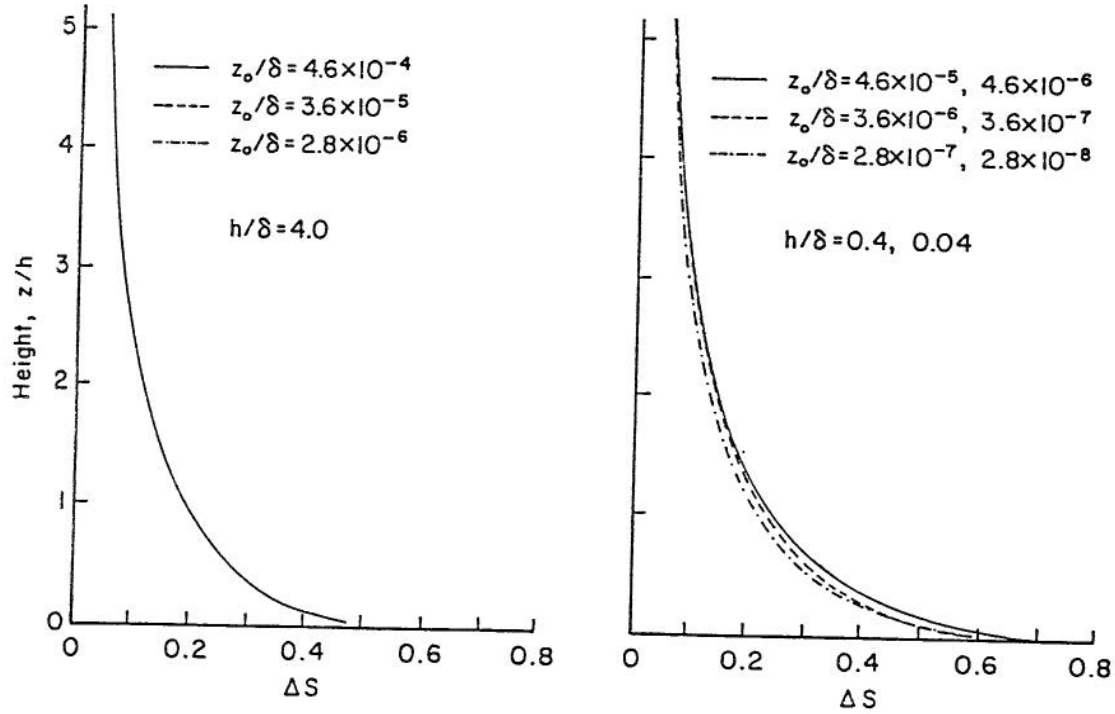

Figure 4.1.4 Fractional speedup ratios predicted from numerical inviscid flow calculations (Bouwmeester *et al.*, 1978)

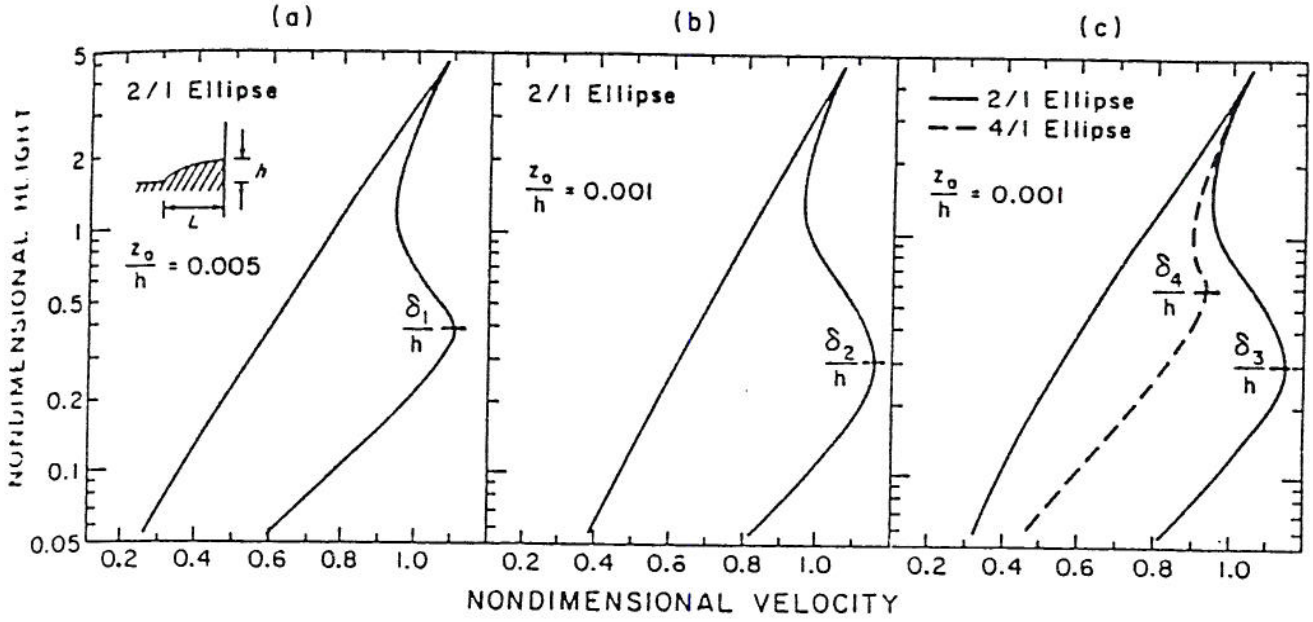

Figure 4.1.5 Flow over elliptical obstacles. Heights are scaled by object height. Velocities are scaled by upstream velocity at z/h = 3. (Jensen and Petersen, 1978)

but from Equation [3.5.4] we can argue $l_z / z_o \approx (L/z_o)^{0.8}$, so

$$\Delta S(z) = (h_{hill} / L)\sigma(x) \, (\ln[L/z_o]/(0.8 \ln[L/z_o]))^2 \neq f(z_o). \qquad [4.1.2]$$

Thus, most analysis predicts that variation in homogeneous surface roughness upwind and over the hill will produce only small changes in the fractional speedup, but consequently large variations in the actual mean profiles.

4.2 Change in Roughness Effects on Flow Over Hills/Mountains

An early observation made during wind-tunnel measurements was that when surface roughness was reduced over the steeper models the mean velocity on the lee side actually increased, and the flow did not separate, even intermittently, though the flow remained turbulent. Conventional wisdom for flow around bluff bodies usually proposes the addition of surface roughness to inhibit separation not its removal. Britter et. al. (1981) explained this paradox by arguing that the delay of separation is induced because the surface velocity near the separation point is increased as the flow accelerates over the smoother hill surface. Thus the boundary layer can penetrate further into the adverse pressure gradient on the lee side of the hill. (The boundary layer is energized by the descent of streamlines toward the wall after a decrease in surface roughness.)

4.2.1 *Linear-perturbation Model Insights*

Jensen and Petersen (1978) discussed the possibility of adding the linear-perturbation solutions for boundary layer response to changes in surface roughness and elevation. Since the solutions are separately linear their perturbations should be additive; thus

$$u(z)_{\text{hill \& roughness}} = u_o(z) + \Delta u(z)_{\text{roughness}} + \Delta u(z)_{\text{hill}}. \qquad [4.2.1]$$

Hunt (1978) applauded this step, and he concluded that the maximum perturbation induced by change of roughness would occur at height z_{o2} whereas the maximum perturbation induced by the hill would occur at height l_z. Consequently, it is not really possible to cancel out the changes induced by one effect by the other. Hunt proposed the ratio:

$$\frac{|\Delta u(l_z)_{hill}|}{|\Delta u(z_{o2})_{rough}|} = \frac{(h_{hill}/L)(\ln[L/z_{o1}])^2}{\ln[l_z/z_{o2}]\ln[z_{o2}/z_{o1}]} \qquad [4.2.2]$$

Thus, where there is a large change in roughness of say 1 m to 10 cm at the hill half-width, if it is accompanied by a change in slope say 1 in 4 over a hill width of 1000 m, the maximum hill slope effect is comparable to the change in roughness effect! On the other hand, if the change of roughness is from 2 m to 2 cm under otherwise similar conditions, then the maximum hill slope effect is five times less than the maximum roughness effect!

4.2.2 *Field and Fluid Model Data*

Britter et al. (1981) performed wind-tunnel experiments over a polynomial shaped hill for which h = 0.1 m, L = 0.25 m, z_o = 0.002 m, and u_* / U_δ = 0.0685. The authors suggested that at a model scale of 1: 500 the surface roughness corresponded to a value of about 1 m (forest canopy). A second experiment was performed where the roughness ended 1 m upwind of the hill crest. This resulted in significant acceleration in the lower part of the boundary layer as a direct result of the change in roughness as shown in **Figure 4.2.1.** Finally, velocity profiles were also measured at the equivalent location of the hill crest downwind of the roughness change after the hill was removed. Examination of the figure reveals that the increase in wind speed of the smooth hill over the rough hill is almost exactly equal to the perturbation induced by the change in roughness alone.

4.3 Laboratory Measurements of Vegetation Covered Terrain

Extensive tree shelter belts were planted over the Rakaia Gorge, NZ, terminal moraine and river plain studied by Meroney et al. (1978). These 10 m high dense tree belts were planted by farmers to protect sheep paddocks. Comparison of field and physical model measurements revealed that the shelter belts played a dominant role in determining near surface winds. Measurements made over vegetation free models of the Rakaia Gorge over-estimated wind speeds and under-estimated turbulence levels at a 10 m measurement height **(Compare Figures 4.2.2, 4.2.3, 4.2.4 and 4.2.5).** When vegetation was modeled field and laboratory wind speeds agreed at sample correlation coefficient levels from 0.68 to 0.78 and rank correlation coefficient levels from 0.78 to 0.95. (Sample correlation coefficient levels for field measurements at the same sites taken on independent days was only 0.68. This suggests that there is an inherent limitation to the paired replication of any single realization of a wind flow pattern by an model whether physical or numerical.

Recently Gong and Ibbetson (1989) reported physical model measurements made over cosine shaped hills and ridges of slope 15°. They added a uniform roughness to the hills made of a rubber sheet having flat-topped circular cylinders 3 mm high and 2 mm diameter at a uniform spacing of 3.6 mm between centers. The surface Reynolds number, Re_* , was about 5 ,which implies a rough model surface during simulations. Hill height was 31 mm and half hill width was 100 mm. The effective surface roughness, z_o, was determined to be 0.17 mm. If we assume a scale ratio of 1:10,000 then field scale hill height would be 310 m, roughness height would be 30 m, and surface roughness, z_o, equals 1.7 m. This would be typical of many forest covered hills/mountains found in nature. Gong and Ibbetson recorded extensive mean velocity, shear, and turbulence information. Comparisons of their data against linear-perturbation models was excellent on upwind hillsides and higher levels. Measurements over the two-dimensional ridge and the circular hill suggests that the mean flow and turbulence over a circular hill resembles those over two-dimensional ridges of similar cross-section, but with reduced perturbation amplitudes.

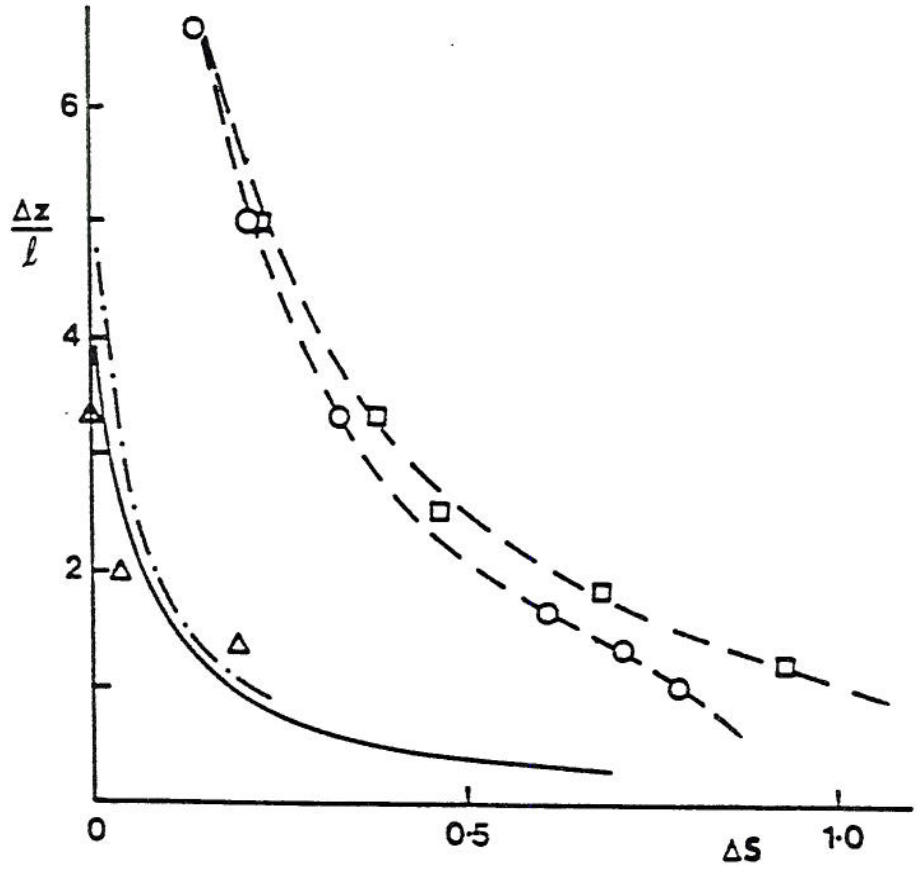

Measured fractional speed-up ΔS ($= \Delta u/U_0$) at top of the smooth and rough hills.

△ roughness change, no hill
—○— rough hill
—□— smooth hill
— · — (smooth) – (rough) hill
——— Townsend roughness change theory

Figure 4.2.1 Measured fractional speed-up at top of the smooth and rough hills. (Britter *et al.*, 1981)

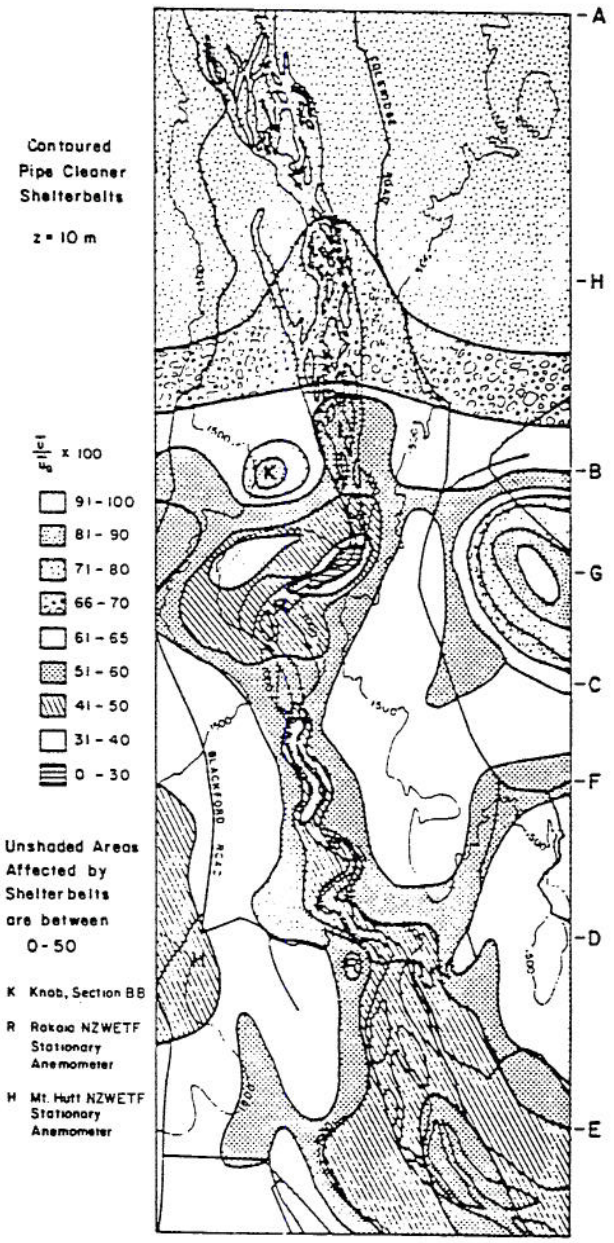

Figure 4.2.2 Horizontal isotachs over Rakaia Gorge, N.Z. z_p = 10 m. (Meroney *et al.*, 1978)

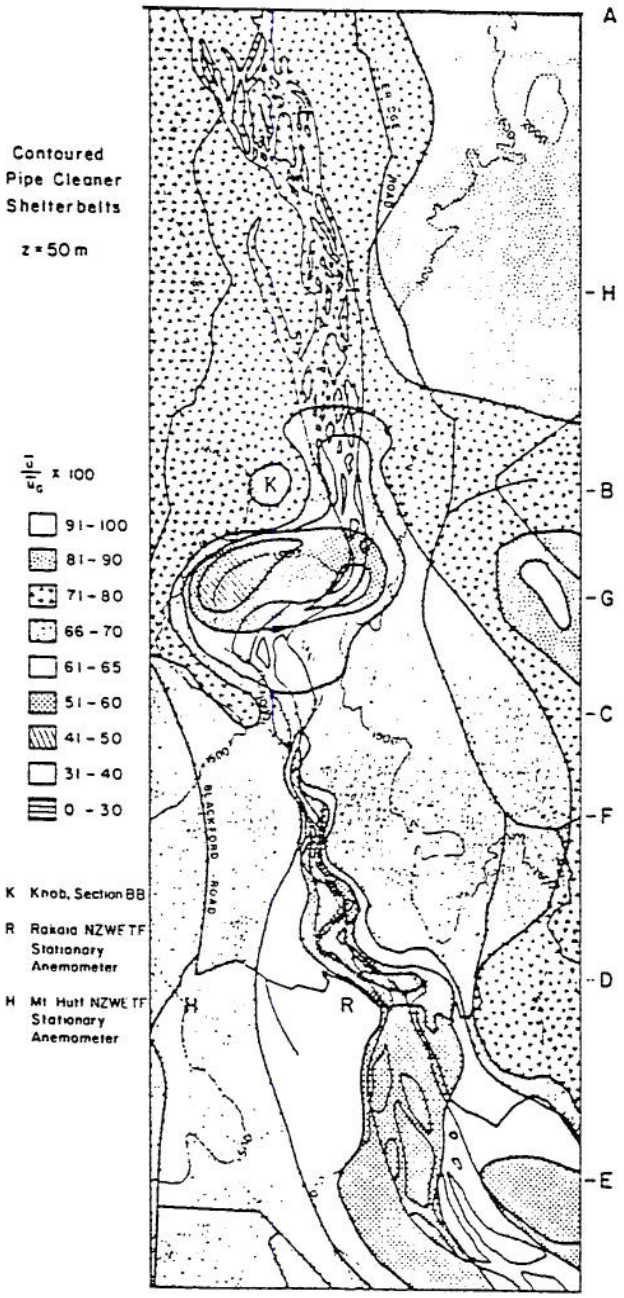

Figure 4.2.3 Horizontal isotachs over Rakaia Gorge, N.Z., z_p = 50 m. (Meroney *et al.*, 1978)

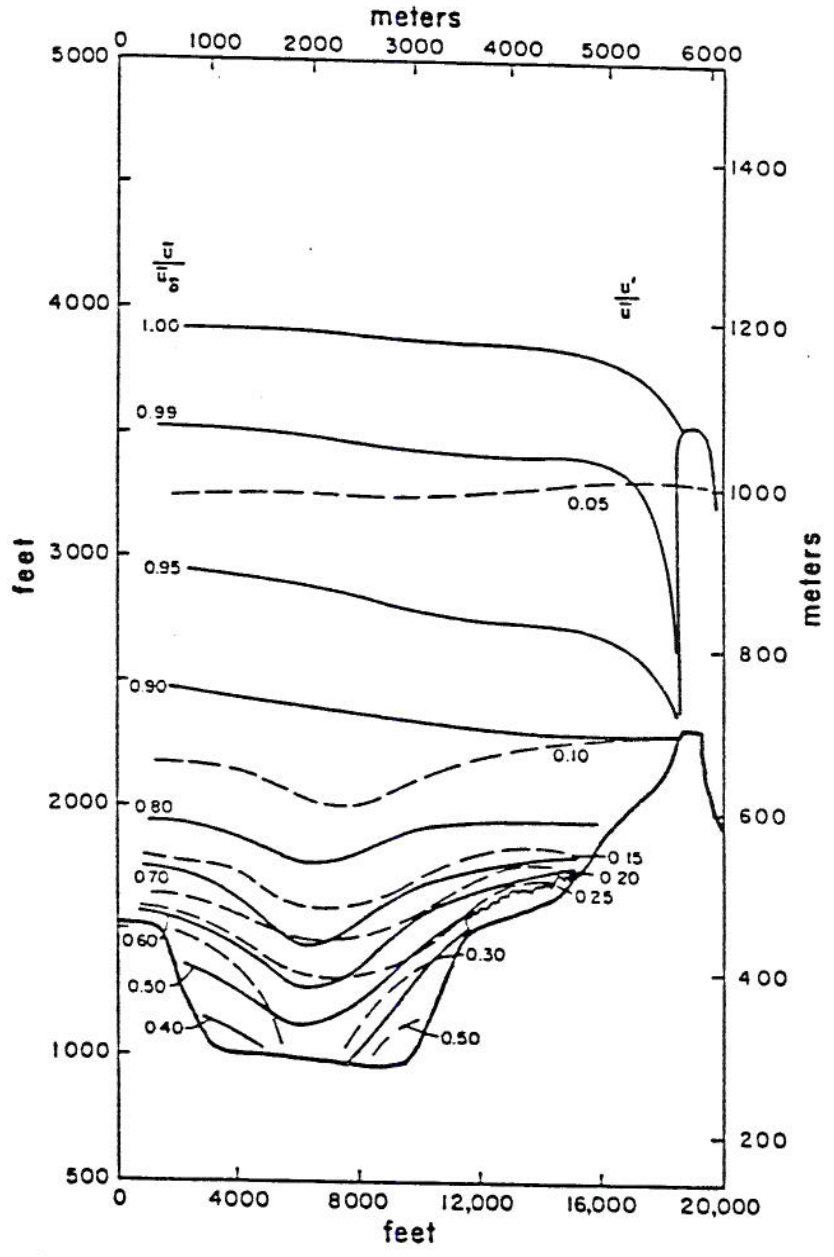

Figure 4.2.4 Vertical section G-G isotachs at Rakaia Gorge, N.Z. (Meroney *et al.*, 1978)

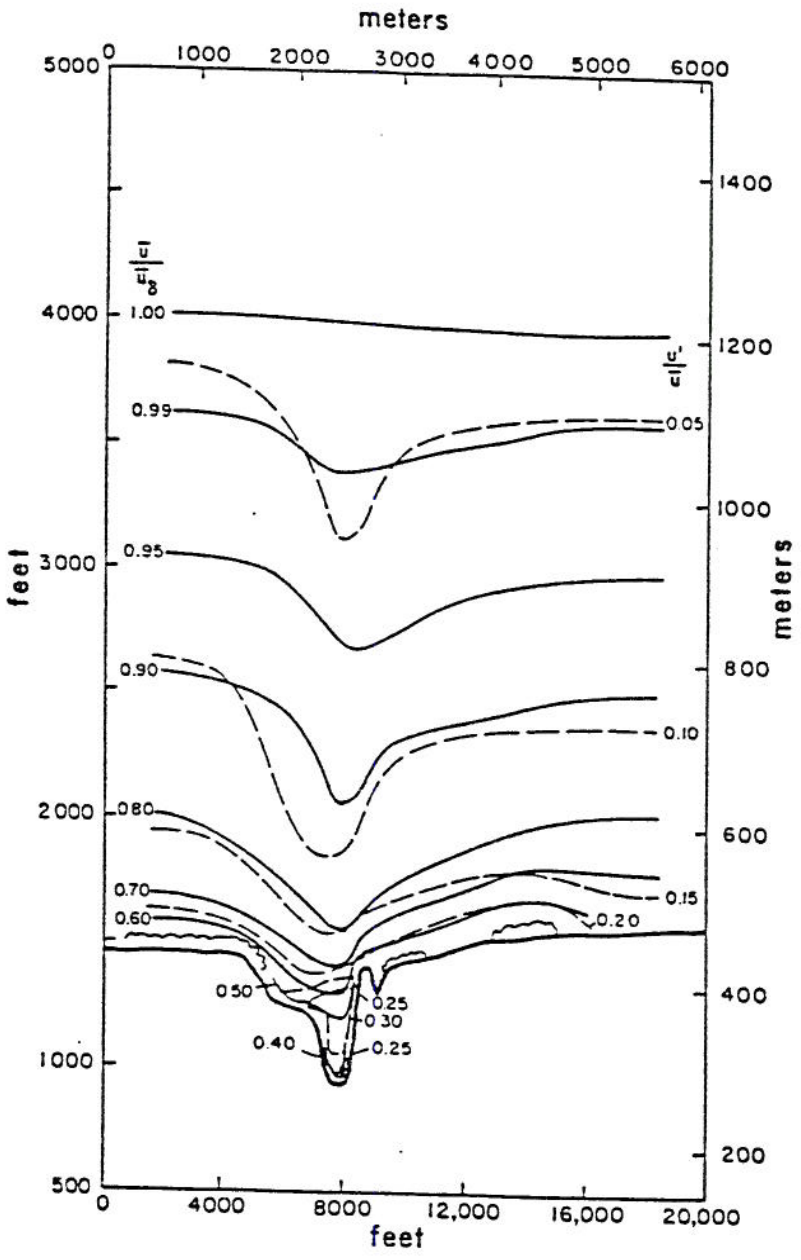

Figure 4.2.5 Vertical section F-F isotachs at Rakaia Gorge, N.Z. (Meroney *et al.*, 1978)

4.4 Summary

The removal of vegetation upwind of the crests of hills has been shown to substantially increase hill-top winds and reduce the probability of separation and consequent gustiness. Most evidence available from fluid model studies. Models based on linear-perturbation principles appear to predict correctly the order of magnitude of combined elevation and roughness change effects on wind speed profiles. Inviscid flow models are not expected to account for the effects of roughness change over hilly terrain.

V. ANALYTIC AND NUMERICAL MODELS

Today there are literally dozens of numerical models available to predict various aspects of flow over complex terrain. Both the use of linear and primitive equation models for flows over complex terrain are discussed in Blumen (1990). A review and classification of complex terrain models was prepared by Meroney (1990) for the Forest Service. Prediction codes or algorithms for flow over complex terrain can grouped into those designed to describe situations where a) stratification causes flow to divert around or over hills and mountains, b) flows which are diverted, accelerated or decelerated due to variations in surface contours, temperature, and roughness in the absence of separation or recirculation, or c) flows where backflows and recirculation may occur as a result of obstacle separation, valley drainage circulations, land/water recirculations, etc. Parallel with these flow categories one can identify at least six categories of numerical modeling:

i) Dividing streamline models,
ii) Phenomenalogical models,
iii) Mass-consistent or objective analysis models,
iv) Depth integrated models,
v) Linear-perturbation models, and
vi) Full primitive equation models.

It would not be appropriate to review all complex terrain models here. A comprehensive list of models by name, type and author will be provided in Appendix tables. Prominent members of each that have been applied to the vegetated terrain problem will be described to identify the advantages and disadvantages of each approach. Copies of almost all model source codes are available by request or purchase. Dividing streamline, depth integrated (shallow layer), and phenomenalogical models have primarily been used to predict plume dispersion in stratified flow situations associated with hill/plume interaction or valley drainage flows. Hence, they will not be considered further here.

5.1 Mass-consistent or Objective Analysis Models Applied to Vegetation Covered Terrain

This class of models combines some objective (regression or maximizing or minimizing some variable) analysis of available wind data to form a wind field. The wind field analysis typically forces the resulting flow to satisfy air mass continuity by constraining the flow between the ground surface and some elevated inversion height. Such models may either produce a fully three-dimensional wind field, or they may solve the depth integrated continuity equation in a horizontal plain, and then recreated a vertical field assuming certain similarity profiles. Comments about specific numerical characteristics of different mass-consistent models are reserved for Appendix Section 2.0. Appendix Table A.1 lists several objective analysis models potentially suitable for wind energy analysis.

5.1.1 *NOABL Predictions for Clearcut Effects Over Cape Blanco, Oregon*

Lin, Veenhuizen, and Qualmann (1985) ran hybrid 2-D and 3-D numerical models for estimating wind flow in Cape Blanco area of Oregon. The effects of terrain height and vegetation were examined. Model was calibrated against kite anemometers. Winter and summer seasonal flows were simulated using long-term wind data at eight fixed height anemometers. The authors report that the variance between measured and predicted winds was only 10%. Results of simulation show that presence of forest in wind turbine site area could cause substantial vertical and horizontal wind shear. Computer simulations were used to assess the impact of tree removal, and they found typical increases of 6 mph at 40 feet and 4 mph at 100 feet above ground.

Veenhuizen and Lin (1982) looked at a 2-dimensional model for flow over a simulated clearing. Subsequently, Veenhuizen and Lin (1983) examined the Goodnoe Hills, WA, area by using a surface roughness length smoothing scheme. They adjusted for the presence of trees by using a virtual origin shift associated with the height of the tree canopy where $d = 0.6\ h$ and a specified roughness length, $z_o = 0.25\ (h-D)$ where $u/u^* = 5.75 \log[(z-d)/z_o)]$. Note that this gives $u/u^* = 5.75 \log[\ 10(z-0.6h)/h]$; hence, the equation is oversimplified because it does not allow for atmospheric stability and tree density. Roughness lengths were specified over test area for forest, scrub, town, swamp, cleared forest, prairie and beach such that z_o varied from 1.52 m to 0.005 m. A system was used to smooth between the forest and cleared areas as noted in **Figure 5.1.1** Basically the method produces a weighted average of roughness lengths based on examining specified roughness lengths from aerial maps around the point of interest. A similar smoothing was used for the displacement lengths.

Horizontal wind fields at a specified height were initially estimated from a 2-dimensional program , then these winds were distributed in the vertical using power law formulae which results in profile predictions shown in **Figure 5.1.2 and 5.1.3.** Once initialized from the estimated profiles NOABL was then used to calculate the final wind fields! Up to 50 iterations were permitted to occur, after which it was assumed wind field was divergence free. Authors provide validation comparisons between short-term measurements and calculations; then they provide comparisons between long-term seasonal measurements and calculations.

Areal distributions of wind speed were calculated for heights of 50, 100 and 200 feet above the ground with isotach plots. Calculations were also made after an assumption of tree removal over potential wind power sites. The authors plotted wind speed difference isotachs for same regions after tree removal. (Unfortunately, the report figures are difficult to read; hence, no example is reproduced here.) Tree removal caused a maximum of +6 mph at 50 feet, but at 200 feet zero wind speed increase occurred.

a. Surface vegetation

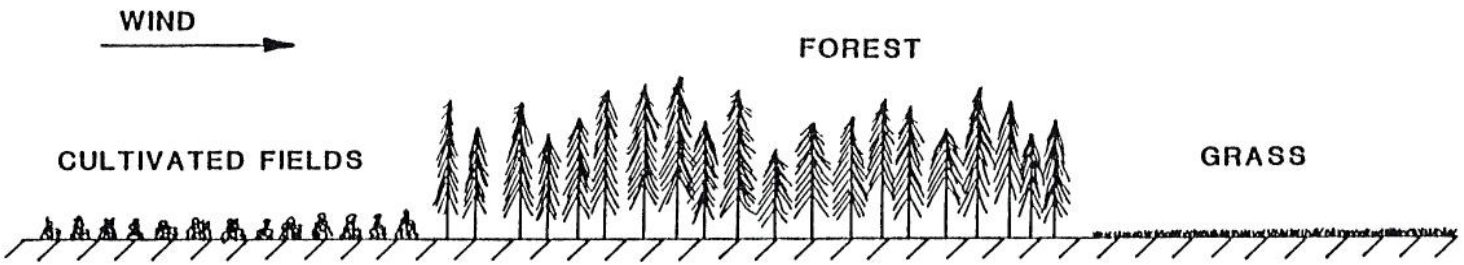

b. Surface roughness length

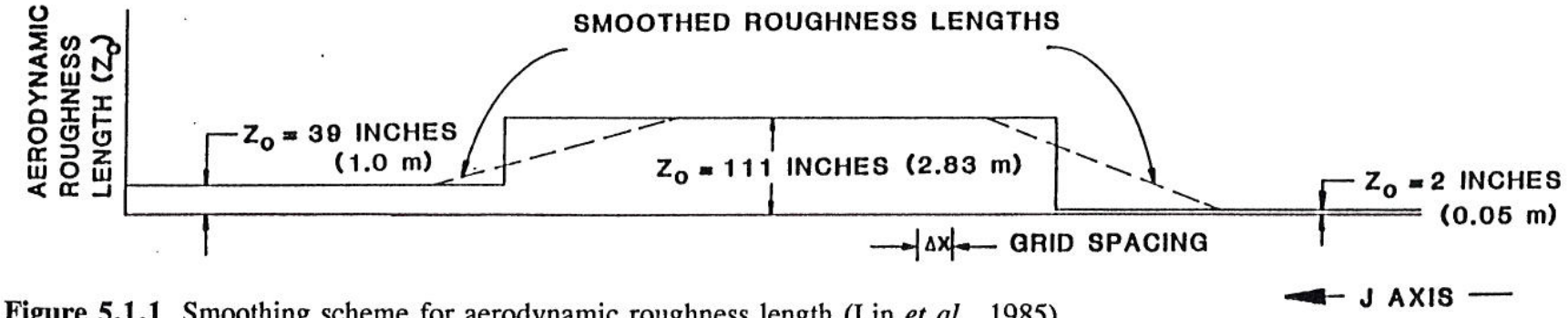

Figure 5.1.1 Smoothing scheme for aerodynamic roughness length (Lin *et al.*, 1985)

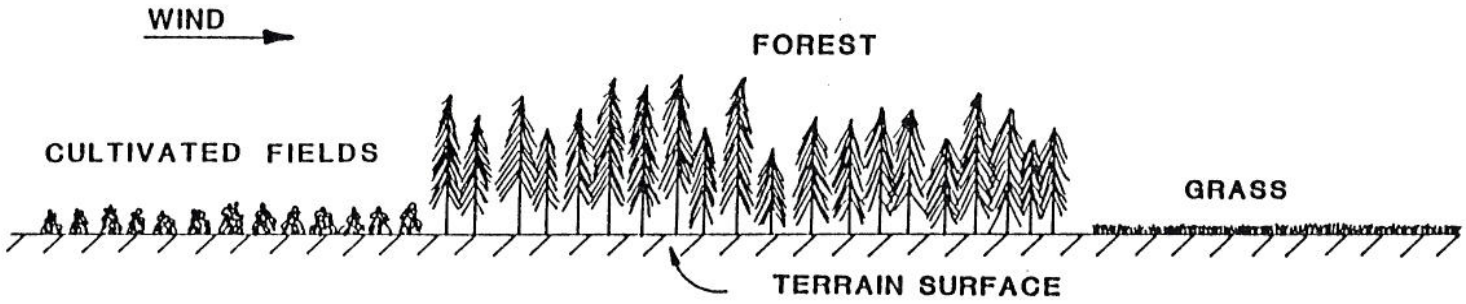

b. Vertical wind profiles, Z_1=200' above the virtual origin shifted surface

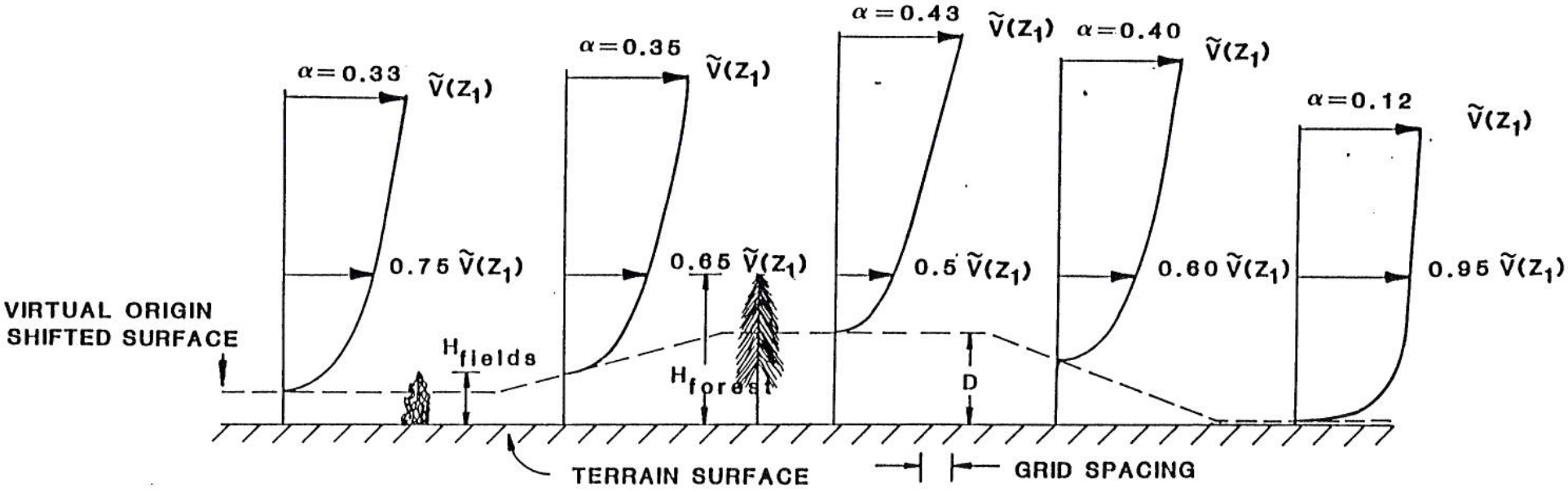

Figure 5.1.2 Vertical wind profiles over a surface of smoothed surface roughness (Lin *et al.*, 1985)

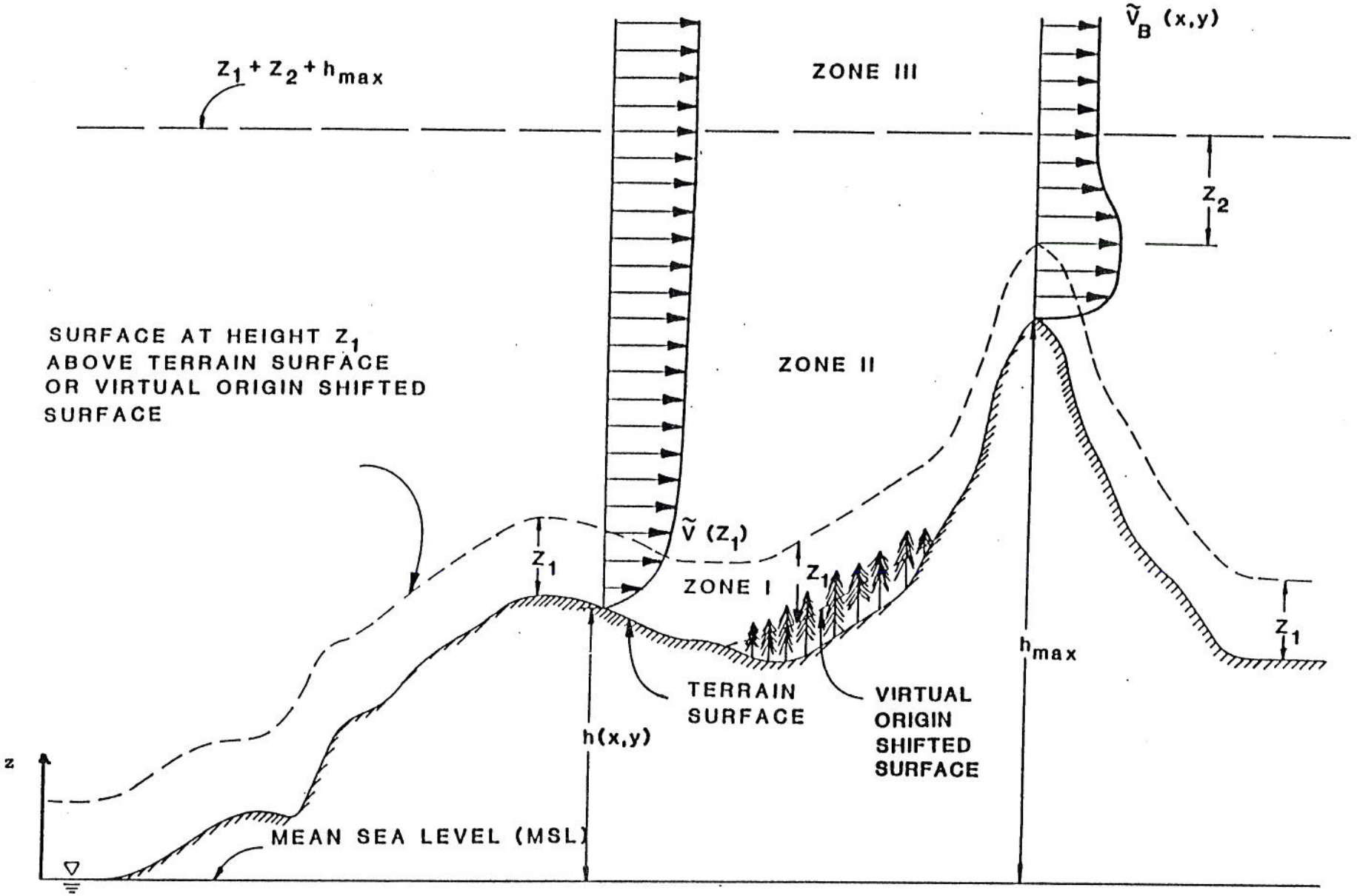

Figure 5.1.3 Initialization of vertical wind profiles for 3-D wind flow computations. (Lin *et al.*, 1985)

Lin (1989) reports the use of the same program to predict the reduction of fugitive dust over coal piles near a power station using wind shelterbelts and wind turbines to reduce surface wind speeds. A wind break model and a turbine wake model was added to the NOABL model. Lin (1990) combined the modified NOABL program, turbine wake model and a turbine performance model to estimate total energy availability for a complex site and distribution of wind turbines. Validation runs were made against field data available for actual wind farms for which wind energy performance was available.

(United Industries Corporation is no longer in business. They turned over their programs and data to R. Lynette and Associates, a consultant firm located in Redmond, Washington. This firm uses program to evaluate complex terrain for wind farm operators, investors, and insurance carriers concerned about low-wind regions used to promote wind energy investments.)

5.1.2 *Atmospheric Science Laboratory (ASL) Model Predictions*

Cionco (1982) and Lanicci (1985) report calculations using the ASL objective analysis model modified to include vegetation. **Figures 5.1.4** and **5.1.5** present a typical complex terrain scenario with grass, forest and villages and the resultant surface-layer wind field produced by the ASL model, respectively. The model appears to account for downslope and vegetation which results in convergence and divergence at a specified height. Cionco combined ASL diagnostic predictions with his own above- and under-canopy algebraic models which allow for specification of vegetative indexes and coupling ratios for different types of cover, **Figure 5.1.6**. The effect of a flow passing from a ten cm tall grass into a 15 m tall forest on a hillside is displayed in **Figure 5.1.7**. The model reproduced subcanopy jetting, lofting of the flow over the canopy wall and subsequent streamline penetration some 10 to 20 tree heights downwind.

Later Lancini used a 3-dimensional extension of the 2-dimensional ASL model to examine a 5 km x 5 km section of Fort Polk Military Reservation in Louisiana. The model was modified to handle the effects of stratification, streamline displacement and variable surface roughness associated with vegetation. The author assumed $d = 0.7\ h_{veget.}$ and $z_o = 0.14\ (h_{veget.} + 0.1)$. The model was used to calculate the effects of vegetation on drainage flows, but no field verification of the predictions were presented.

5.1.3 *NUATMOS Predictions of Complex Terrain Flows*

Ross et al. (1988) describe the mass-consistent model jointly developed by the Chisholm Institute of Technology, Australia, and the Rocky Mountain Forest and Range Experiment Station, Fort Collins, CO. Grandfather of this model is MATHEW and the father is ATMOS1, but the new model has better terrain following boundary conditions, parameters to separately adjust vertical and horizontal wind components, and versions can be run on PC-486 size computers. The RMFRS is currently adapting the model to include vegetative canopies, but the modifications are not yet available. NUATMOS has been "extensively" tested against field data from the CTMD and ASCOT programs. The model appears to correctly predict streamline splitting, plume impaction, and nocturnal drainage flows.

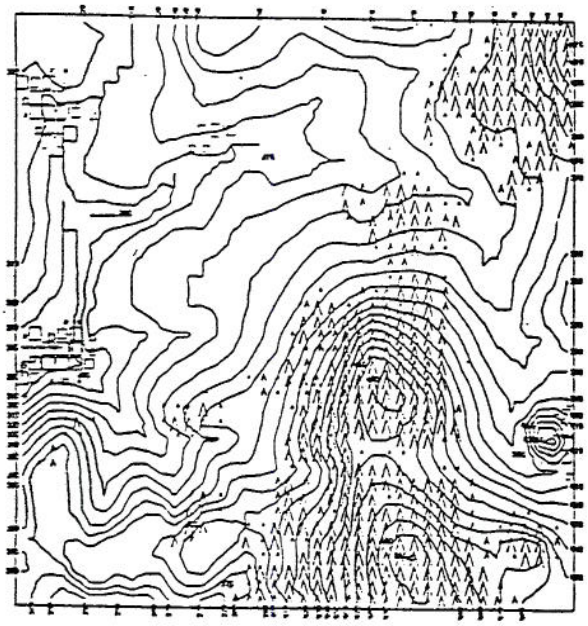

Figure 5.1.4 Typical complex terrain scenario with grass and forest (∧)vegetation and villages (□). (Cionco, 1982)

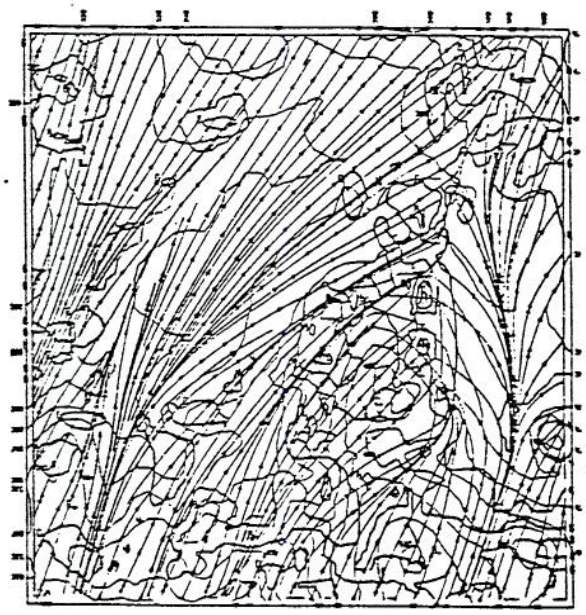

Figure 5.1.5 Surface layer windfield solution for Figure 5.1.4. (Cionco, 1982)

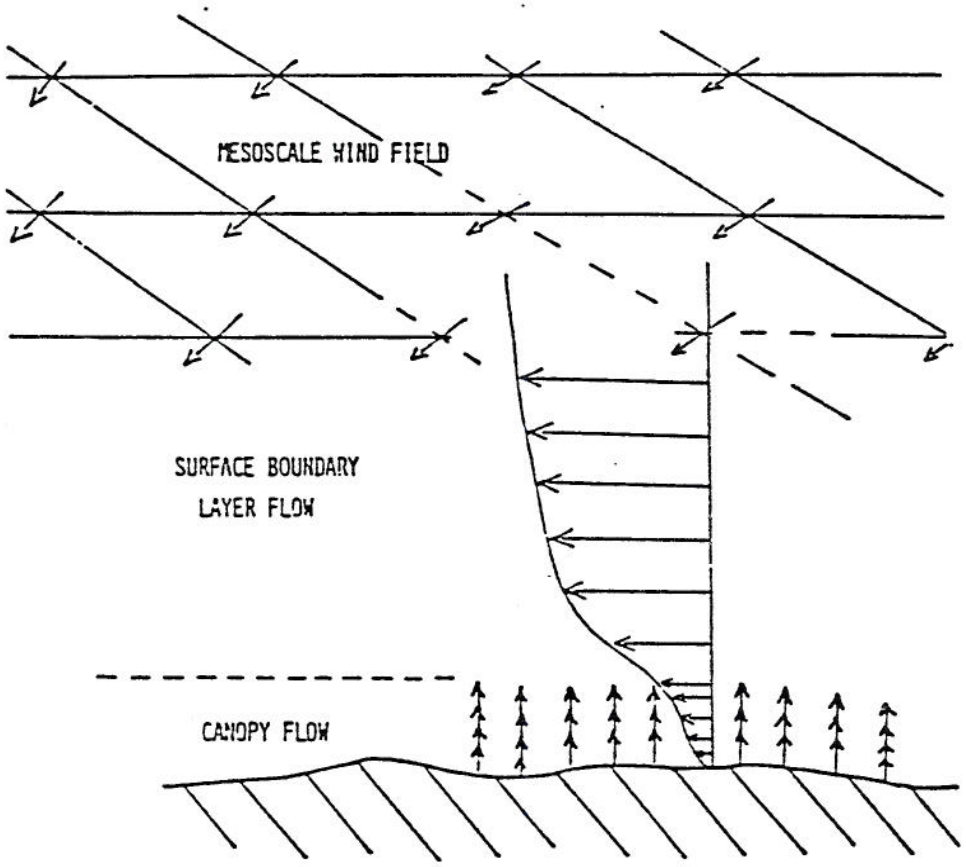

Figure 5.1.6 Schematic of 3-dimensional coupled wind model (Cionco, 1982)

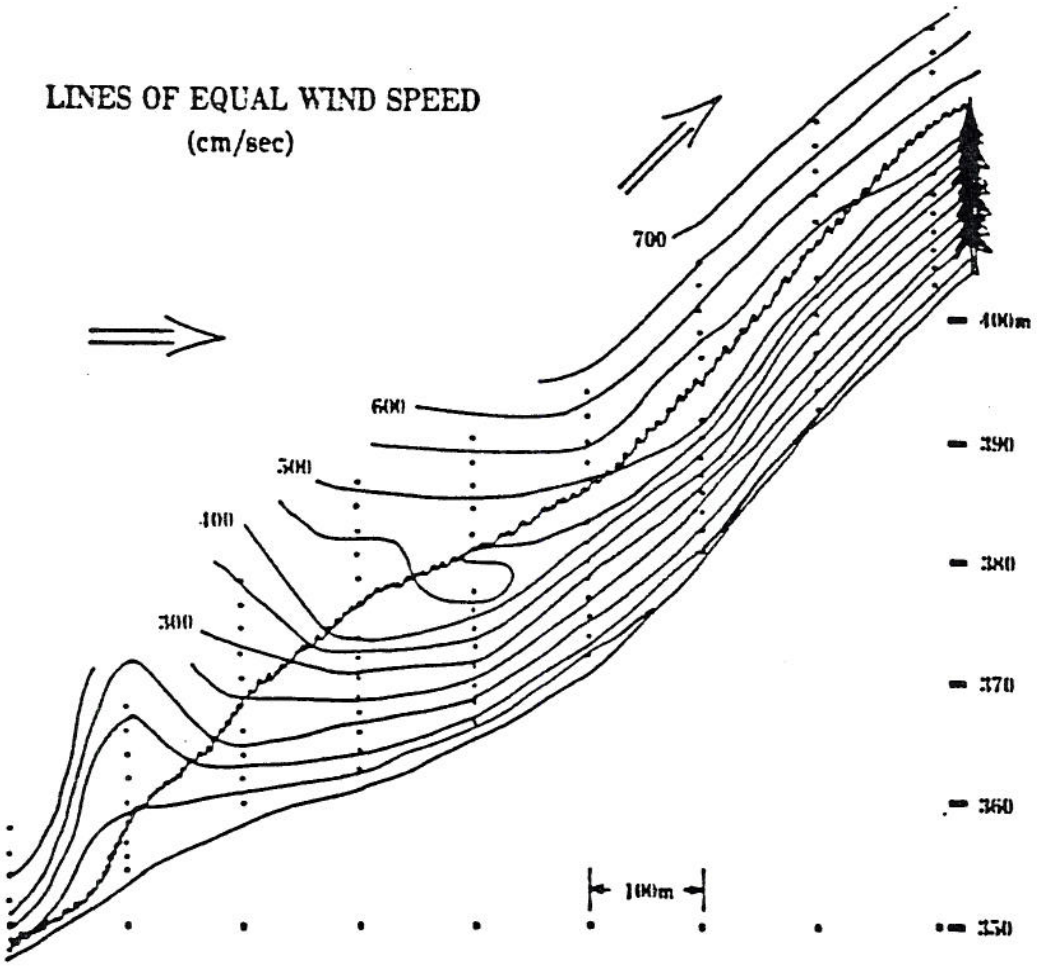

Figure 5.1.7 Cross-section analysis of adjacent grid point wind profiles. (Cionco, 1982)